A Numerical Study on the Edgewise Compression Strength of Sandwich Structures with Facesheet-Core Disbonds

Andrew C. Bergan*
NASA Langley Research Center, Hampton, VA, 23681

Damage tolerant design approaches require determination of critical damage modes and flaw sizes in order to establish nondestructive evaluation detection requirements. A finite element model is developed to assess the effect of circular facesheet-core disbonds on the strength of sandwich specimens subjected to edgewise compressive loads for the purpose of predicting the critical flaw size for a variety of design parameters. Postbuckling analyses are conducted in which an initial imperfection is seeded using results from a linear buckling analysis. Both the virtual crack closure technique (VCCT) and cohesive elements are considered for modeling disbond growth. Predictions from analyses using the VCCT and analyses using cohesive elements are in good correlation. A series of parametric analyses are conducted to investigate the effect of core thickness and material, facesheet layup, facesheet-core interface properties, and curvature on the criticality of facesheet-core disbonds of various sizes. The results from these analyses provide a basis for determining the critical flaw size for facesheet-core disbonds subjected to edgewise compression loads and, therefore, nondestructive evaluation flaw detection requirements for this configuration.

I. Introduction

SANDWICH structures are often used in launch vehicles for their high specific stiffness and strength. Since launch vehicle structures are susceptible to damage from manufacturing defects and impact events, a damage tolerance approach is often used for structural substantiation. In a damage tolerant design, each credible failure mode must have a detectable flaw size that is several times smaller than the critical flaw size, where the critical flaw size is defined as the flaw size that renders the structure unable to carry the design loads.

One particular failure mode that is often of concern for sandwich structures is separation at the facesheet-core interface. Facesheet-core disbonds can occur as a result of manufacturing process errors. When sandwich structures with facesheet-core disbonds are subjected to edgewise compression loads, the disbonded region may exhibit local buckling. If sufficient load is applied, the locally buckled disbond region may propagate, leading to structural failure.

Several authors have studied the facesheet-core disbond failure mode using finite element models with the virtual crack closure technique (VCCT) or cohesive elements to predict facesheet-core disbond growth. Termaath et al. used the VCCT to investigate facesheet-core disbonds in single cantilever beam specimens[1]. VCCT has also been applied to plate structures. Reeder et al. demonstrated a high level of test-analysis correlation for solid laminates with embedded delaminations and loaded under edgewise compression[2]. The test and analysis showed that sublaminate buckling occurs and leads to collapse, which is a response similar to that of sandwich structures with facesheet-core disbonds subjected to edgewise compression. A finite element model with VCCT has also been used to predict facesheet-core disbond growth when the core is pressurized[3]. Han et al. demonstrated the applicability of cohesive elements for predicting the response of sandwich structures with facesheet-core disbonds loaded under edgewise compression[4]. However, the effect of structural parameters such as core thickness, material properties, and facesheet layup on the strength of specimens with facesheet-core disbonds has not been explored.

The purpose of this study is to provide a numerical assessment of the strength of sandwich structures with facesheet-core disbonds subjected to edgewise compression load. A parametric finite element model was developed to examine the effect of a wide range of structural parameters on the criticality of circular disbonds of various sizes. The model assumes that the facesheet-core disbond growth is the only failure mode. Two methods of modeling the facesheet-core disbond growth were used: cohesive elements and the VCCT. This work complements a recent

* Research Aerospace Engineer, Structural Mechanics and Concepts Branch, 8 West Taylor Street, Mail Stop 190, Member AIAA.

assessment of the effect of facesheet-core disbonds on global buckling response[5]. The paper is organized in the following manner. In section II, the finite element model is described, including the geometric configuation, material properties, mesh and boundary conditions. In section III, the results are described and the effect of varying design parameters on disbond propagation is discussed. A summary and concluding remarks are provided in section IV.

II. Finite Element Model Description

A. Configuration

The model configuration was chosen to resemble the standard test for edgewise compressive strength of composite sandwich construction[6], as shown in Fig. 1. In the standard test configuration, a pristine sandwich specimen is tested. In the configuration shown in Fig. 1, a circular disbond is included with diameter *D*. The disbond is placed at one facesheet-core interface. The specimen has a height of 7.9 inches and a width of 5.9 inches. The overall dimensions were selected so that the disbond is not influenced by edge effects. The core and facesheets have thickness t_c and t_f, respectively. The size of the disbond, core thickness, and facesheet thickness were varied parametrically. Abaqus Standard[7] models were generated using python scripts, so that new models with different combinations of model parameters could be easily generated.

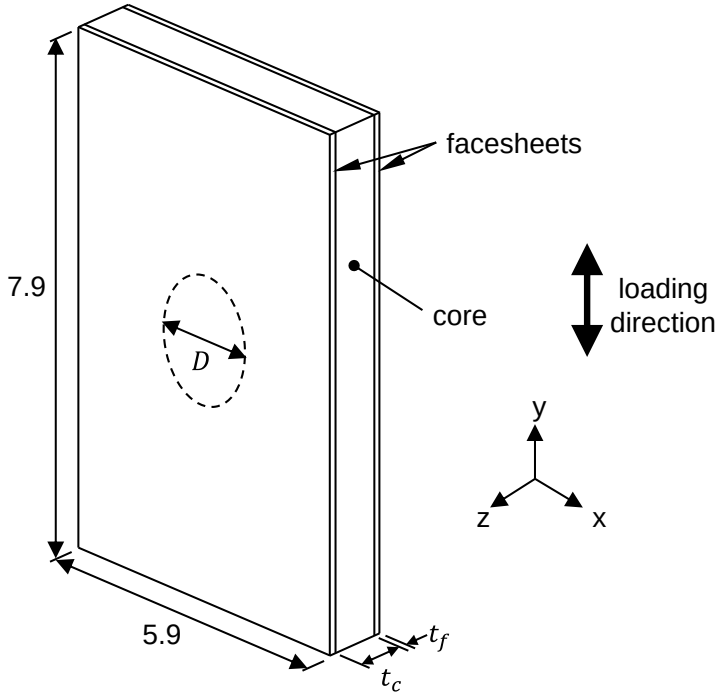

Figure 1. Configuration used for analysis of the critical size of kissing bonds at the facesheet-core interface (All dimensions are in inches).

Under edgewise compressive load, the driving force for initiation and propagation of the disbond is local buckling of the disbonded region. Therefore, the postbuckling analyses are conducted in two steps. In the first step, a linear eigenvalue buckling analysis is performed. The first buckling mode (local buckling of the disbond region) is used to seed an imperfection in the mesh for the subsequent analysis with an amplitude of $0.03t_f$. In the second step, a geometrically nonlinear postbuckling analysis procedure is used where the edgewise compressive load is applied as a prescribed end shortening. The duration of this step was 1.0 unit of pseudo time for all models. Cohesive elements or the VCCT are used to capture growth of the disbond and thus predict the strength of the specimen. This analysis procedure extends the work of Reeder et al. to the case of sandwich constructions.[2]

B. Material Properties

The facesheets are composed of IM7/8552 tape with a 0.0057 inch ply thickness. The elastic material properties are listed in Table 1. Three facesheet layups were considered: $[45/–45/0_2/90]_s$, $[45/-45/0/90]_s$, and $[60/–60/0]_s$ where the 0°-direction is coincident with the loading direction. Multiple core materials, including foam and aluminum honeycomb, were considered. The elastic properties for the core materials are listed in Tables 2 and 3. For the aluminum honeycomb cores, the ribbon direction was aligned with the loading direction.

A variety of methods have been used to measure the fracture toughness for the facesheet-core interface, G_c, resulting in a wide variety of reported values.[8–15] Three values that span the range of measured G_c values for the chosen material systems are considered here: 2.9 lbf/in, 5.7 lbf/in, and 8.6 lbf/in. Mode-independent damage propagation was assumed for the facesheet-core interface using a Mode I value for fracture toughness, which is a conservative assumption since Mode II and mixed-mode fracture toughnesses are typically higher than the Mode I fracture toughness.[14] For the cohesive elements, the strength was assumed to be 1827 psi[15] and the penalty stiffness was calculated following the recommendation by Turon et al.[16]

Table 1. Elastic properties for IM7-8552 facesheet tape.[17]

E_1 [ksi]	E_2 [ksi]	G_{12} [ksi]	ν_{12}
24,860	1320	760	0.32

Table 2. Elastic properties for foam core.[18]

Density [lb/ft^3]	E [ksi]	G [ksi]
6.9	19.7	7.3

Table 3. Elastic properties for aluminum honeycomb core.[5,19]

Density [lb/ft^3]	E_1 [ksi]	E_2 [ksi]	E_3 [ksi]	G_{12} [ksi]	G_{13} [ksi]	G_{23} [ksi]	ν_{12}	ν_{13}	ν_{23}
3.1	21.3	21.3	75	5.3	45	22	1.0E-5	1.0E-5	0.33
4.5	21.3	21.3	150	5.3	70	31	1.0E-5	1.0E-5	0.33

C. Mesh and Boundary Conditions

A typical mesh is shown in Fig. 2. The core and facesheets are represented with one layer of continuum shell elements (SC8R) each. A refined mesh is used in the region near the disbond front and a coarser mesh is used in the far-field region. The typical far-field mesh size is 0.25 inches. For models that use cohesive elements, the mesh size in the refined mesh region is 0.01 inches to satisfy guidelines for cohesive element size.[16] The cohesive elements (COH3D8) are placed in the region highlighted in green in Fig. 2a. The cohesive elements are replaced with tie constraints during the first analysis step (eigenvalue buckling analysis). The typical number of degrees of freedom for the models with cohesive elements is 300,000. For models that use VCCT, a typical refined mesh size of 0.08 inches is used, as established by a mesh convergence study. The typical number of degrees of freedom for the models with VCCT is 60,000. For both models with cohesive elements and models that used the VCCT, a contact condition is used in the second step to prevent the facesheet from penetrating the core within the disbond region. Also, in both models, damage growth is allowed only within the refined mesh region. Once damage propagation reaches the transition region, the model results are truncated, since damage is artificially arrested at this point and, as such, the results are no longer physically meaningful.

The boundary conditions used in the analysis are shown in Fig. 3. The boundary conditions were intended to represent loading between two platens. The free edges were restrained, so that no out-of-plane defection could occur, in order to prevent global buckling.

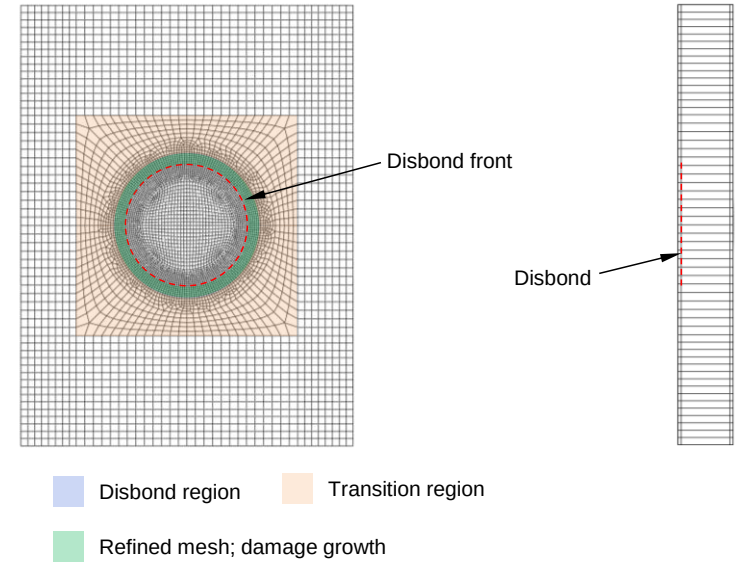

Figure 2. Typical mesh used for the critical disbond size analysis.

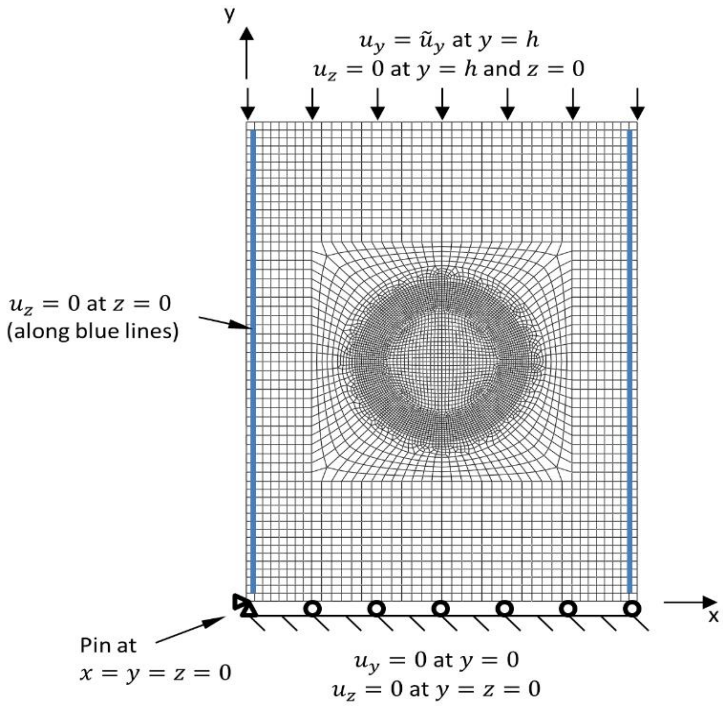

Figure 3. Boundary conditions for the critical disbond size analysis.

III. Results and Discussion

A. Nominal Configuration

Results for the configuration referred to as the nominal configuration are given in this section. The purpose is to highlight the characteristics of the model response and to investigate the impact of selected model assumptions. The nominal configuration has a foam core that is 1.0 inch thick, $[45/–45/0_2/90]_s$ facesheet layup, and G_c = 5.7 lbf/in.

1. Eigenvalue Buckling Analysis

The first mode from the eigenvalue buckling analysis was used to seed an imperfection in subsequent postbuckling analyses. A typical contour plot of the imperfection displacement field in the z-direction for the first eigenmode is shown in Fig. 4 for a 1.6-inch disbond size. It is observed that the disbonded region buckles outward in the positive z-direction. All other configurations resulted in similar deformation patterns.

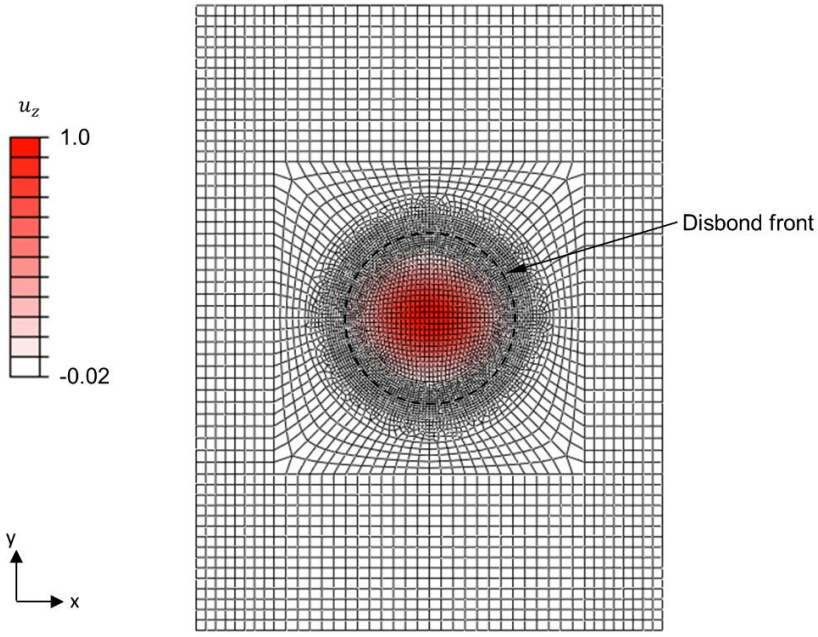

Figure 4. Typical first eigenmode of the buckling analysis.

2. Postbuckling Analysis

The results of postbuckling analyses using the VCCT and cohesive elements were compared to assess the consistency of the two modeling approaches. Typical load-displacement responses, damage propagation, and deformation are shown in Fig. 5 for a model with cohesive elements and in Fig. 6 for a model with VCCT. In both cases, the models had an initial disbond size of 1.6 inches. Three key points in the load-displacement response are designated in Fig. 5: damage initiation (I), onset of load-displacement nonlinearity (N), and peak load (P). The damage state and out-of-plane displacement are shown as contour plots for each key point in the load-displacement history. It is observed that when the peak load (P) is reached, damage has propagated to a critical length. Similarly, the peak load (P) point is highlighted and corresponding contour plots of the damage state and out-of-plane displacement are shown in Fig. 6. The VCCT prediction does not indicate damage initiation prior to the peak load.

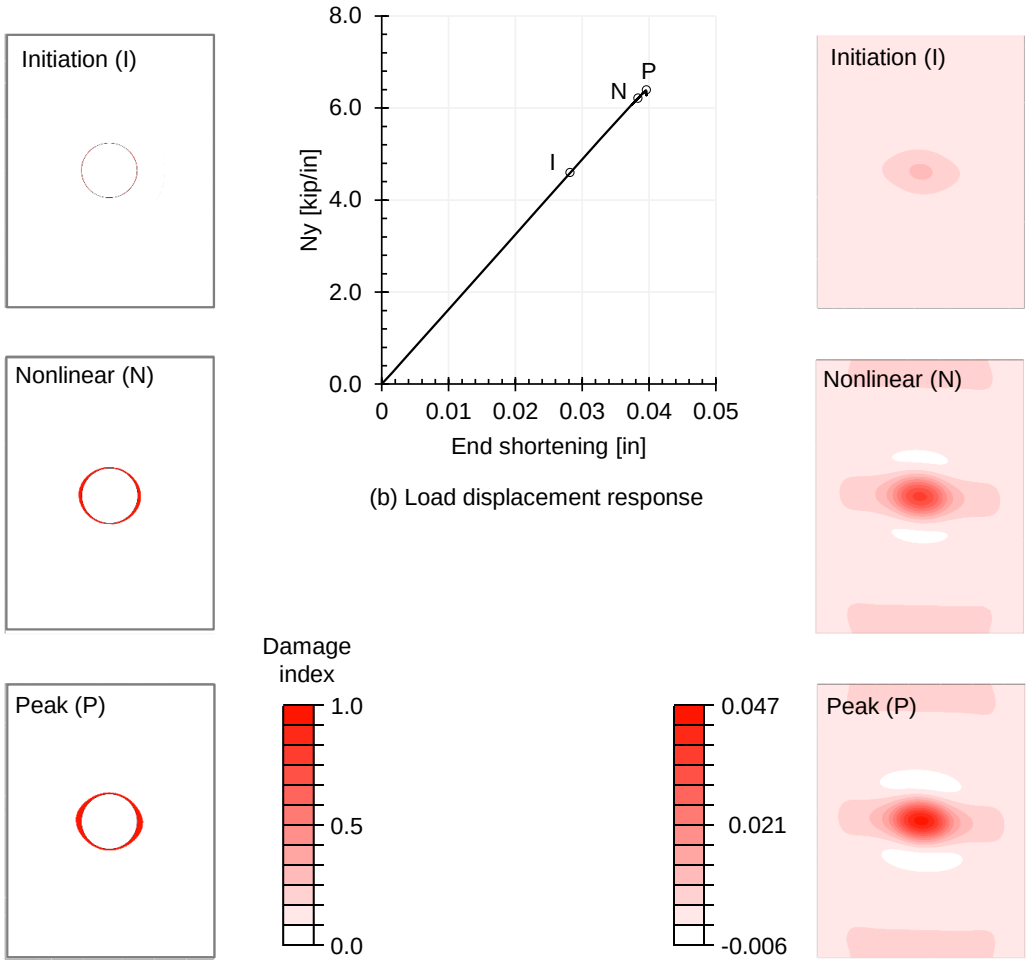

(a) Damage propagation states

(b) Load displacement response

(c) Displacement states for u_z [in]

Figure 5. Damage, load-displacement response, and out-of-plane deformation predicted using cohesive elements.

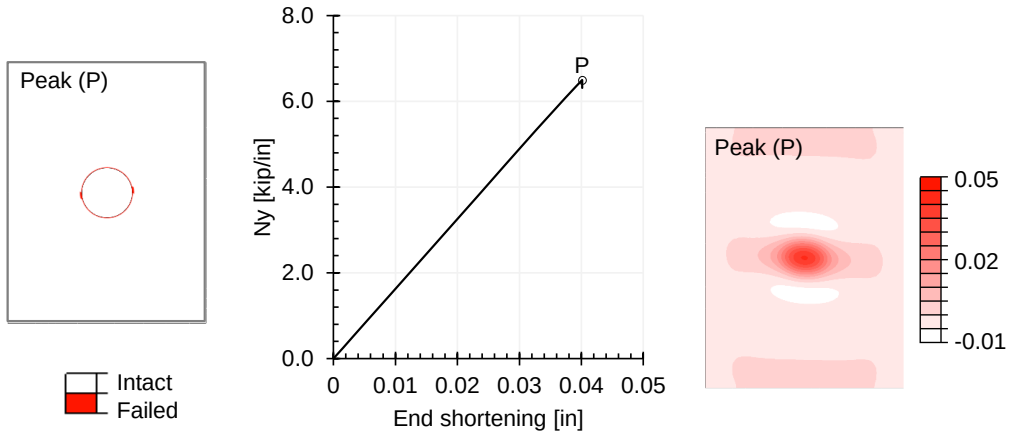

(a) Damage propagation

(b) Load displacement response

(c) u_z [in]

Figure 6. Damage, load-displacement response, and out-of-plane deformation predicted using VCCT.

In contrast to the prediction using cohesive elements, the model with VCCT does not capture damage initiation and initial accumulation, but it does capture damage propagation after the peak load. Differences between the predictions from the two fracture mechanics approaches are expected due to the fact that the VCCT approach is based on a linear elastic fracture mechanics formulation while the cohesive elements consider both strength and fracture through a nonlinear fracture mechanics formulation. While the model using the VCCT provides less insight into the damage process compared with the model using cohesive elements, the model using the VCCT requires only 20% of the computational time of the model with cohesive elements. The difference in computational expense between the two models is due to two factors: 1) the difference in the number of degrees of freedom in the models and 2) the cohesive element model suffers from more extensive load-incrementation convergence difficulties than the VCCT model.

Both models using cohesive elements and models using the VCCT require the analyst to specify solution parameters that can have a significant impact on the results. For the VCCT model, a contact stabilization parameter of 1×10^{-6} was used as recommended by Krueger.[20] Trial and error showed that larger values of this parameter and automatic selection of this parameter by Abaqus yielded varying results that were in poor agreement with the predictions from the model with cohesive elements. For the model with cohesive elements, viscous regularization was used to limit the convergence difficulties. A viscous regularization coefficient of 1×10^{-6} was found to provide a good balance between improving convergence and having a minimal effect on the load-displacement response. Increasing the viscous regularization coefficient beyond the value selected resulted in a rounded load-displacement response that overshoots the peak load instead of a sharp load drop. Models with smaller values of the viscous regularization coefficient converged significantly more slowly and resulted in a similar load-displacement response. Though both solution parameters (contact stabilization parameter and viscous regularization coefficient) are the same, this is likely a coincidence for the particular structure considered here. It is assumed that the solution parameters established here are valid for the range of model configurations considered. Different structures may require different solution parameters.

The representation of the core with one layer of continuum shell elements (SC8R) was compared with a higher fidelity representation that included several layers of solid elements (C3D8R). Since transverse shear stresses and deformations are important in the disbond propagation process, there was a concern that the continuum shell representation of the core would not yield accurate results. The models that represented the core with continuum shell elements underpredicted the peak load compared with the models that represented the core with solid elements by 2.5% and 4.2% for VCCT and cohesive elements, respectively. Since the differences between the two representations were quite small, the subsequent analyses used continuum shell elements to represent the core in order to take advantage of the lower computational expense.

3. Critical Size of Facesheet-Core Disbond

The disbond size was varied to obtain the load carrying capability as a function of disbond size. The results are shown in Fig. 7 as predicted by the linear eigenvalue buckling analysis, the postbuckling analysis using cohesive elements, and postbuckling analysis using VCCT. The results indicate that the models using cohesive elements and VCCT are in good agreement for the range of disbond sizes considered. The eigenvalue buckling analysis underpredicts the load carrying capability when the disbond is large. However, the eigenvalue buckling analysis is useful as a quick and conservative preliminary design tool for assessing the severity of this failure mode.

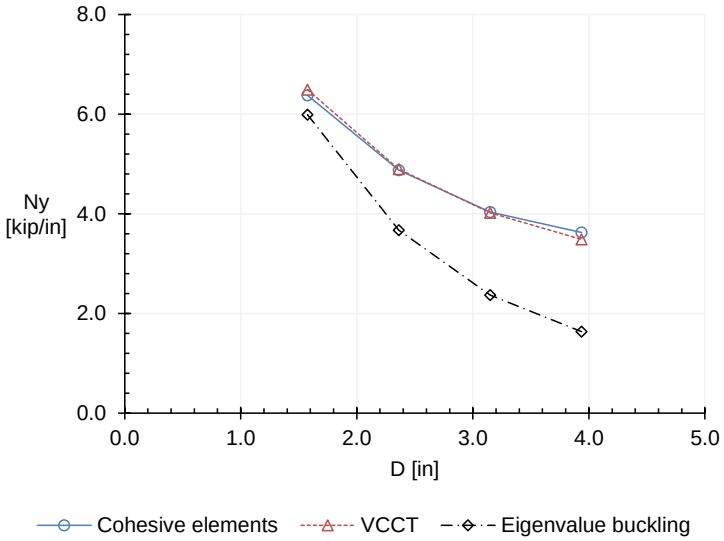

Figure 7. Critical disbond size.

The results shown in Fig. 7 suggest that the VCCT method is an appropriate technique for further evaluating the effect of several

parameters on load carrying capability.

B. Parametric Studies

Model parameters including t_c, G_c, the facesheet layup, core material, and curvature were varied to highlight the relevant significance of each on the predicted response. Since certain combinations of model parameters excited other failure modes (global buckling and facesheet wrinkling), an additional boundary condition, $u_z = 0$ for $z = 0$, was introduced to ensure that the dominant failure mode is facesheet-core disbond growth. Since the VCCT approach yielded peak load predictions in good agreement with the cohesive element based models, the VCCT approach was used for the parametric studies. All models used the nominal configuration with the exception of the parameters that were varied parametrically.

1. *Effect of Core Thickness and Material*

The core thickness of 0.25 inch, 0.5 inch, 1.0 inch (nominal), 1.5 inch, and 2.0 inch were considered for a range of initial disbond sizes. The results for the 1.0 inch, 1.5 inch, and 2.0 inch core thicknesses are shown in Figure 8a. The results for the 0.25 inch and 0.5 inch core thicknesses were nearly identical to the nominal 1-inch thickness and so these results are not shown in Figure 8a. It was found that increasing the core thickness had a very minor strengthening effect. The core material had a more substantial impact on the model response, as shown in Figure 8b, where there is a significant different between the aluminum honeycomb cores (red and green curves) and the foam core (blue curve) for small disbond sizes. For an initial 1.6-inch-diameter disbond, the 4.5 pcf aluminum honeycomb had a 42% higher strength than the foam core. The sensitivity to the core material is likely a result of the difference in transverse shear stiffnesses of the different materials.

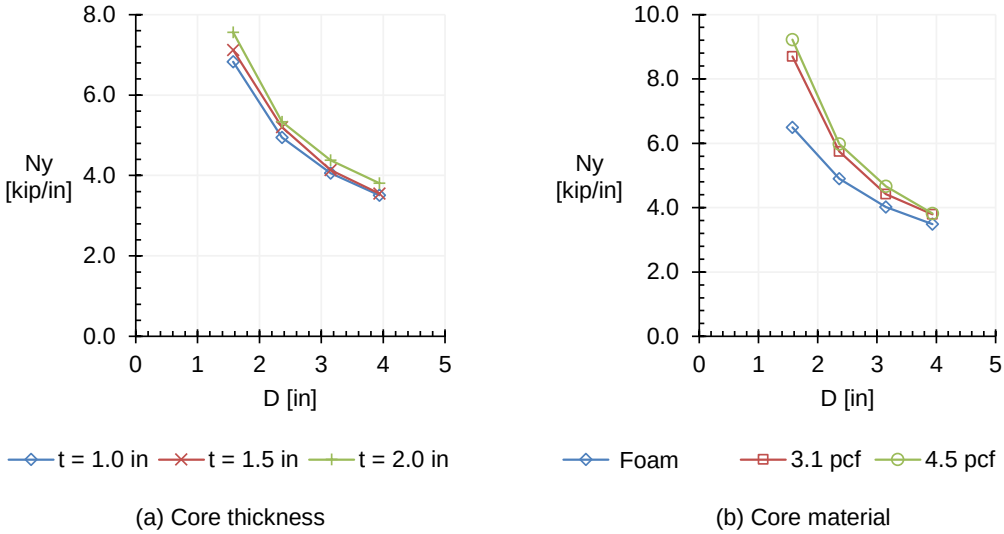

(a) Core thickness (b) Core material

Figure 8. Effect of core thickness and material.

2. *Effect of Interface Fracture Toughness*

Three values for interface fracture toughness were considered: 2.9 lbf/in, 5.7 lbf/in (nominal), and 8.6 lbf/in. A relatively consistent trend of increasing strength with increasing fracture toughness was observed across a range of initial disbond sizes and core thicknesses, as shown in Figure 9. The G_c values of 2.9 lbf/in and 8.6 lbf/in were considered lower and upper bounds for the set of materials considered here and so the corresponding results can be considered to define the envelope of the expected responses in light of uncertainty in the value of G_c.

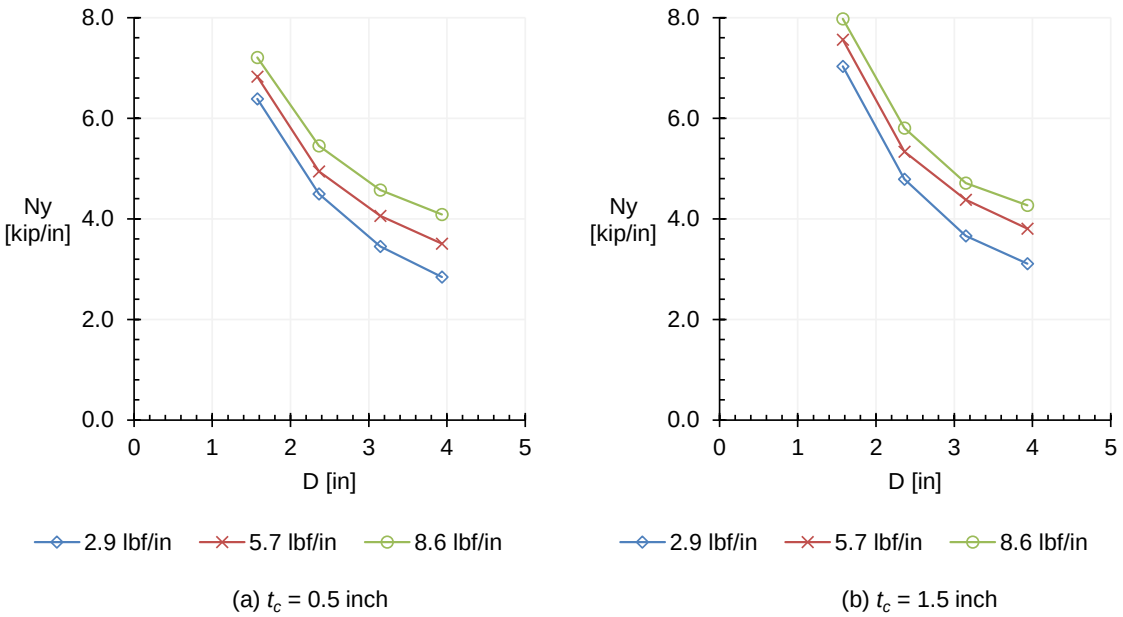

Figure 9. Effect of interface fracture toughness.

3. Effect of Facesheet Layup

Three facesheet layups were considered and the results for each layup are shown in Figure 10. The propensity for a facesheet to buckle has a large impact on the results. For instance, relatively stiff layups have similar responses. In contrast, a softer layup has a significantly lower strength across the range of disbonds considered.

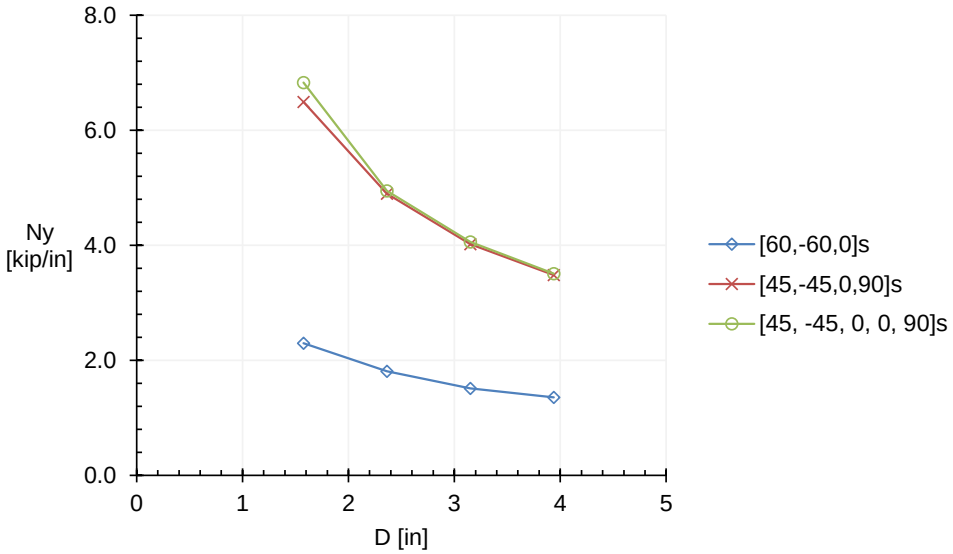

Figure 10. Effect of facesheet layup.

4. Effect of Curvature

Curvature generally has a significant effect on global buckling response. The effect of curvature was examined to determine the significance of curvature on the localized disbond. The predicted strengths for a range of radius of curvatures, ρ, normalized to the sandwich thickness, t, are shown in Figure 11. The disbonded interface was considered on the convex surface and concave surface, independently. It is observed that there is very little change in strength for the relatively large curvatures considered. For larger disbonds and smaller radii of curvature,

disbonds located on the convex surfaces sustain slightly higher load levels than structures with disbonds located on the concave surfaces.

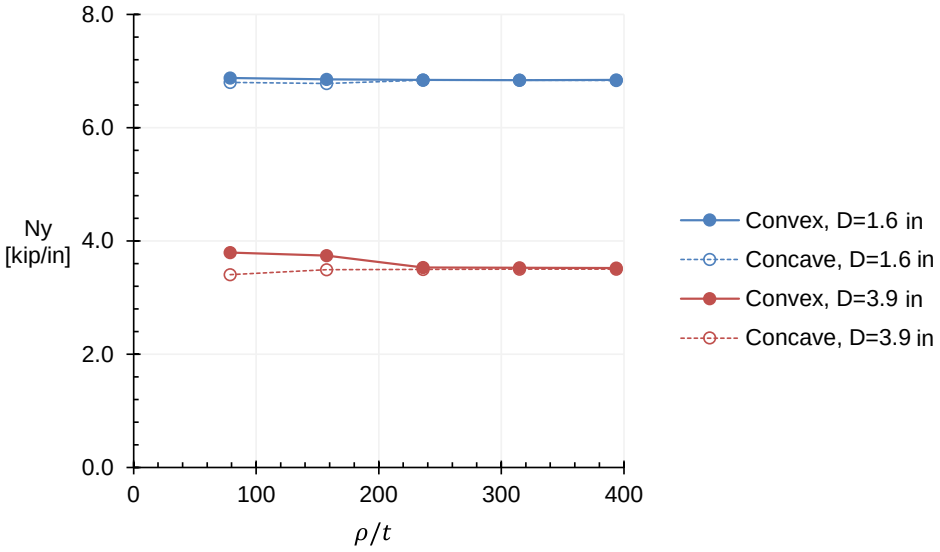

Figure 11. Effect of curvature.

IV. Conclusion

A numerical assessment was conducted to investigate the effect of facesheet-core disbonds on the strength of sandwich specimens subjected to edgewise compression loads. A parametric finite element model was developed for this purpose. Two approaches were used to represent growth of the facesheet-core disbond: the virtual crack closure technique (VCCT) and cohesive elements. The results from the two approaches were compared, highlighting the modeling requirements, sensitivity to solution parameters, and predicted response for each. Good agreement was found between the two modeling approaches for peak load prediction.

The parametric finite element model was exercised to investigate the effect of core thickness and material, facesheet layup, facesheet-core interface toughness, and curvature on disbond growth. The VCCT approach was chosen for these parametric studies since it is less computationally expensive. It was found that the strength varied significantly with core material, facesheet layup, and interface fracture toughness for a given disbond size. In contrast, the core thickness and curvature had relatively insignificant effects on strength. These results provide insight into the relative strength of a variety of common sandwich configurations with a range of facesheet-core disbond sizes and can be used to aid in definition of flaw size detection requirements for nondestructive evaluation.

References

[1] Termaath, S. C., Ingraffea, A. R., and Wawrzynek, P. A., "A Computational Fracture Mechanics Approach for the Analysis of Facesheet-from-Core Disbond of Honeycomb Core Sandwich Panels," *Fatigue and Fracture Mechanics: 30th Volume*, West Conshohocken, PA: ASTM International, 2000, pp. 169–182.

[2] Reeder, J. R., Chunchu, P. B., Song, K., and Ambur, D. R., "Postbuckling and Growth of Delamination in Composite Plates Subject to Axial Compression," *43rd AIAA/ASME/ASCE/AHS/ASC Structures, Structural Dynamics, and Materials Conference*, Denver, CO, Apr. 2002.

[3] Glaessgen, E. H., Reeder, J. R., Sleight, D. W., Wang, J. T., Raju, I. S., and Harris, C. E., "Debonding Failure of Sandwich-Composite Cryogenic Fuel Tank with Internal Core Pressure," *Journal of Spacecraft and Rockets*, vol. 42, 2005, pp. 613–627.

[4] Han, T.-S., Ural, A., Chen, C.-S., Zehnder, A. T., Ingraffea, A. R., and Billington, S. L., "Delamination Buckling and Propagation Analysis of Honeycomb Panels Using a Cohesive Element Approach," *International Journal of Fracture*, vol. 115, May 2002, pp. 101–123.

[5] Pineda, E. J., Myers, D. E., Bednarcyk, B. A., and Krivanek, T. M., "A Numerical Study on the Effect of Facesheet-Core Disbonds on the Buckling Load of Curved Honeycomb Sandwich Panels," *American Society for Composites 30th Technical Conference*, East Lansing, MI, Sept. 2015.

[6] "ASTM Standard C364. 'Standard Test Method for Edgewise Compressive Strength of Sandwich Constructions,'" *Annual Book of ASTM Standards*, W. Conshohocken, PA: ASTM Int., 2012.
[7] *ABAQUS Online Documentation: Version 6.14*, Providence, RI: Dassault Systèmes Simulia Corporation, 2014.
[8] Rinker, M., Ratcliffe, J. G., Adams, D. O., and Krueger, R., "Characterizing Facesheet/Core Disbonding in Honeycomb Core Sandwich Structure," NASA/CR-2013-217959, NASA Langley Research Center, Hampton, VA, Feb. 2013.
[9] Nelson, J. O., "Characterizing Mode I Strain Energy Release Rate Associated with Interfacial Debond Growth in Sandwich Composites," PhD Thesis, University of Utah, Salt Lake City, UT, 2012.
[10] Rinker, M., John, M., Zahlen, P. C., and Schäuble, R., "Face Sheet Debonding in CFRP/PMI Sandwich Structures under Quasi-Static and Fatigue Loading Considering Residual Thermal Stress," *Engineering Fracture Mechanics*, vol. 78, Dec. 2011, pp. 2835–2847.
[11] Ratcliffe, J. G., and Reeder, J. R., "Sizing a Single Cantilever Beam Specimen for Characterizing Facesheet–Core Debonding in Sandwich Structure," *Journal of Composite Materials*, vol. 45, Dec. 2011, pp. 2669–2684.
[12] Østergaard, R. C., Sørensen, B. F., and Brøndsted, P., "Measurement of Interface Fracture Toughness of Sandwich Structures under Mixed Mode Loadings," *Journal of Sandwich Structures and Materials*, vol. 9, Sep. 2007, pp. 445–466.
[13] Nettles, A. T., *Measuring Core/Facesheet Bond Toughness in Honeycomb Sandwich Structures*, NASA/TP-2006-214713, NASA Marshall Space Flight Center, Huntsville, AL, Dec. 2006.
[14] Grau, D. L., Qiu, X. S., and Sankar, B. V., "Relation between Interfacial Fracture Toughness and Mode-mixity in Honeycomb Core Sandwich Composites," *Journal of Sandwich Structures and Materials*, vol. 8, May 2006, pp. 187–203.
[15] Ural, A., Zehnder, A. T., and Ingraffea, A. R., "Fracture Mechanics Approach to Facesheet Delamination in Honeycomb: Measurement of Energy Release Rate of the Adhesive Bond," *Engineering Fracture Mechanics*, vol. 70, Jan. 2003, pp. 93–103.
[16] Turon, A., Dávila, C. G., Camanho, P. P., and Costa, J., "An Engineering Solution for Mesh Size Effects in the Simulation of Delamination Using Cohesive Zone Models," *Engineering Fracture Mechanics*, vol. 74, Jul. 2007, pp. 1665–1682.
[17] Camanho, P. P., Maimí, P., and Dávila, C. G., "Prediction of Size Effects in Notched Laminates Using Continuum Damage Mechanics," *Composites Science and Technology*, vol. 67, Oct. 2007, pp. 2715–2727.
[18] *Qualification report Rohacell 71 HERO*, QTR-2014-RC-MOB-002 iss.1, Evonik Industries AG, Theodore, AL, 2014.
[19] *Hexweb™ Honeycomb Sandwich Design Technology*, AGU 07b, Hexcel Composites, Duxford, UK, Dec. 2000.
[20] Krueger, R., "A Summary of Benchmark Examples to Assess the Performance of Quasi-Static Delamination Propagation Prediction Capabilities in Finite Element Codes," *Journal of Composite Materials*, vol. 49, Nov. 2015, pp. 3297–3316.